Inorganic Chemistry

pubs.acs.org/IC

Article

Periodic Trends in Intra-ionic Excited State Quenching by Halide

Matthew J. Goodwin, Alexander M. Deetz, Paul J. Griffin, and Gerald J. Meyer*

Cite This: *Inorg. Chem.* 2024, 63, 15772−15783

Read Online

ACCESS | Metrics & More | Article Recommendations | Supporting Information

ABSTRACT: The preassociation of reactants in a photoinitiated redox reaction through the use of noncovalent interactions can have a significant impact on excited state reactivity. As these noncovalent interactions render some stabilization to the associated species, they impact the kinetics and thermodynamics of photoinitiated electron transfer. Reported herein is a novel iridium(III) photocatalyst, equipped with an anion-sensitive, amide-substituted bipyridine ligand, and its reactivity with the halides (X = I^-, Br^-, Cl^-) in acetonitrile and dichloromethane. A noteworthy periodic trend was observed, where the size and electron affinity dramatically altered the observed photoredox behavior. The binding affinity for the halides increased with decreasing ionic radius (K_{eq} ~10^3 to >10^6) in a polar medium but association was stoichiometric for each halide in a nonpolar medium. Evidence for the static quenching of iodide and bromide is presented while dynamic quenching was observed with all halides. These results highlight how the photophysics of halide adducts and the thermodynamics of intra-ionic photo-oxidation are impacted as a consequence of preassociation of a quencher through hydrogen bonding.

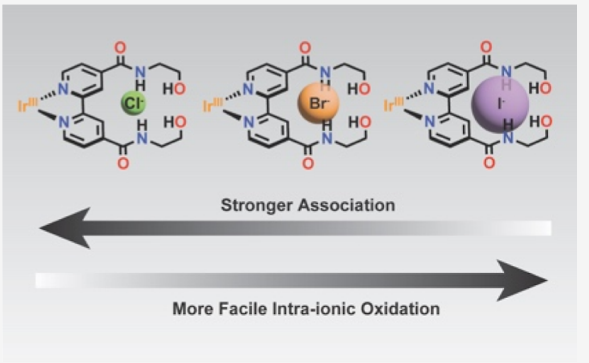

INTRODUCTION

Halides are of great importance to science and technology with emerging applications in solar energy conversion and photochemistry.[1−3] Examples include high efficiency perovskite solar cells where halides are involved in solar light harvesting and carrier transport[4,5] or in dye-sensitized[6−8] or HX splitting[9−13] solar cells undergoing redox chemistry. In addition, halide electron transfer reactivity has been utilized by the photoredox community to drive new synthetic transformations that yield high value organic compounds.[14−34] Optimization of halide chemistry and redox behavior could enhance these applications yet a recent literature review revealed that our quantitative knowledge is largely limited to aqueous solutions and to the gas phase[1] despite many of the applications requiring the use of organic solvents. This is surprising given that the limited data available from measurements made under nonaqueous conditions reveal a marked sensitivity of halide chemistry to the external environment.[35] This may emanate from the belief that the one-electron oxidized halides, the halogen atoms, may extract H atoms from the solvent. However, studies of iodide and bromide oxidation in acetonitrile solutions for applications in dye-sensitized solar cells show that this is not always the case.[1,6−8] Less persistent halogen atoms like $Cl^•$ have been stabilized with aromatic solvents or additives.[26,36−41] Therefore, there is considerable literature precedence indicating that the reactivity of halogen atoms can be controlled in organic solvents. Herein are reported fundamental light induced redox studies of halide association and oxidation by an inorganic photocatalyst in polar and nonpolar organic solvents.

An important predictor of halogen reactivity is their ability to donate an electron.[1−3] The gas phase electron affinities of the halogens of interest herein are given in Scheme 1. A rarely recognized fact is that one-electron halogen potentials, $E^\circ(X^{•/-})$, cannot be obtained by standard electrochemical techniques and are usually determined computationally or through kinetic measurements.[35,42−47] Here too, the impact of the local coordination environment on the one-electron halogen potentials is of keen interest. An example with relevance to this manuscript is the realization of a photocatalyst that selectively associates and photo-oxidizes a halide ion present in a complex mixture such as seawater.[9,48] Such a photocatalyst would need to possess functional groups that recognize and bind halide ions. Clues to how this might be accomplished exist in the anion recognition literature, where it has been shown that hydrogen bonding moieties can effectively associate halides.[49−67] However, the large equilibrium constants (10^{12} to 10^{17}) suggest that the sequestered chloride ions would be far more difficult to oxidize than those freely diffusing in the solution mixture. To this end, studies to understand how association impacts halide photo-oxidation can improve their use in the aforementioned applications.

Received: April 27, 2024
Revised: July 19, 2024
Accepted: July 31, 2024
Published: August 9, 2024

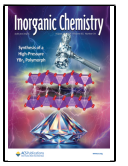

https://doi.org/10.1021/acs.inorgchem.4c01726
Inorg. Chem. 2024, 63, 15772−15783

Scheme 1. Halide Series Studied and Their Respective Atomic Radii and Electron Affinities[1]

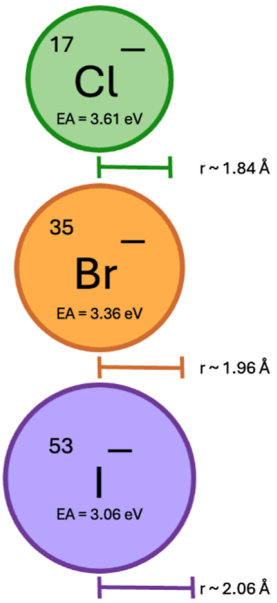

Scheme 2 shows a novel Ir photocatalyst designed to associate halides using an amide-based hydrogen bonding

Scheme 2. Proposed Associative Equilibrium between Ir-dea and Halides

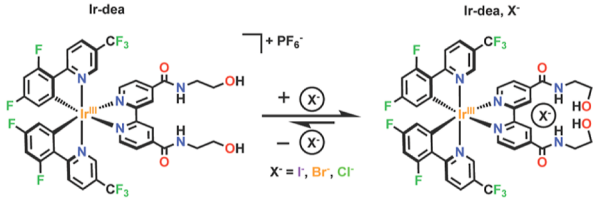

moiety, similar to those previously shown to sense anions.[65] In addition, the monocationic charge of the photocatalyst provides a Coulombic incentive for halide association. Indeed, spectroscopic and X-ray crystallographic data show that the halides do form strong adducts with these H-bonding receptors. Time resolved kinetic measurements provide a useful comparison of how these noncovalent interactions impact intra-ionic photo-oxidation relative to freely diffusing halide ions. In addition, halide association is shown to impact the lifetime and free energy stored in the excited state of the Ir photocatalyst. Taken together, the halide periodic trends provide keen insights into the interplay between ground state halide association and excited state electron transfer.

EXPERIMENTAL SECTION

Materials. The following reagents were used as received unless otherwise stated: acetonitrile (CH_3CN, Burdick & Jackson, spectrophotometric grade, 99.9%); dichloromethane (CH_2Cl_2, HPLC grade, VWR); ethanol (CH_3CH_2OH, VWR); methanol (CH_3OH, VWR); pentane ($CH_3CH_2CH_2CH_2CH_3$, VWR), hexanes (VWR); sulfuric acid (95.0−98.0%, ACS grade, VWR); ethanolamine (98%, BTC); deionized water; argon gas (Airgas, >99.998%); [2,2′-bipyridine]-4,4′-dicarboxylic acid (98%, Ambeed); di-μ-chlorotetrakis[3,5-difluoro-2-[5-trifluoromethyl-2-pyridinyl-κN)-phenyl-κC]diiridium(III) ($[Ir(dF\text{-}(CF_3)\text{-}ppy)_2(\mu\text{-}Cl)]_2$, Strem, ≥99%); ammonium hexafluorophosphate (NH_4PF_6, Sigma-Aldrich); dichloromethane-d_2 (Cambridge Isotope Laboratory) and acetonitrile-d_3 (Cambridge Isotope Laboratory) were stored with 3 Å molecular sieves and stored in a desiccator equipped with Drierite). Tetrabutylammonium hexafluorophosphate, iodide, bromide, and chloride ($TBAPF_6$, TBAI, TBABr, TBACl, Sigma-Aldrich) were all recrystallized from acetone and diethyl ether twice before use and stored in a nitrogen atmosphere glovebox. No uncommon hazards were found in the reported experimentation.

Synthesis. *[Ir(dF-(CF_3)-ppy)$_2$(dea)][PF_6] (**Ir-dea**).* Synthesis of the ligand 4,4′-diethanolamide-2,2′-bipyridine (**dea**) was performed via a modified literature procedure.[68] $[Ir(dF\text{-}(CF_3)\text{-}ppy)_2(\mu\text{-}Cl)]_2$ (50 mg, 0.0336 mmol) and **dea** (25 mg, 0.0757 mmol) were suspended in ∼6 mL of MeOH and added to a 10 mL Anton-Parr microwave reactor vial with a magnetic stir bar. The suspension was microwaved for 2 h at 100 °C. After the reaction completion, the vial contained a yellow solution and some off-white precipitate and was then filtered through Celite to remove excess ligand. An excess of sat. NH_4PF_6 (∼6 mL) was added to the filtrate to crash out the product as the PF_6 salt. The solvent was evaporated and the solid was resuspended/dissolved in water and more sat. NH_4PF_6 (∼2 mL) was added. Dichloromethane was added to the suspension (∼20 mL) yielding a bright yellow organic layer and a very faint yellow aqueous layer. The organic layer was collected and solvent evaporated. The bright yellow solid was redissolved in minimal DCM and was recrystallized with hexanes. The recrystallized product was collected and dried yielding **Ir-dea** as the PF_6 salt (70 mg, 77% yield). ^{1}H NMR (400 MHz, CD_3CN): δ 8.99 (s, 2H), 8.51 (dd, J = 8.86, 2.8 Hz, 2H), 8.21 (dd, J = 8.85, 1.56 Hz, 2H), 8.15 (d, J = 5.68 Hz, 2H), 7.86 (dd, J = 5.72, 1.72 Hz, 2H), 7.71 (s, 2H), 7.64 (app. t, J = 5.01 Hz, 2H), 6.83 (ddd, 12.80, 9.34, 2.33 Hz, 2H), 5.87 (dd, 8.49, 2.35 Hz, 2H), 3.71 (q, 5.54 Hz, 4H), 3.55 (q, 5.58 Hz, 4H), 2.99 (t, 5.68 Hz, 2H). ^{19}F NMR (377 MHz, CD_3CN): δ −64.45 ($-CF_3$), −73.08 (d, PF_6^-), −106.15 (dd, ppy-F), −108.93 (td, ppy-F). ^{13}C{^{1}H} NMR (101 MHz, CD_3CN): δ 167.3 (d, J_{C-F} = 7.49 Hz), 165.8 (dd, J = 204.7, 13.3 Hz), 163.2, 161.1 (dd, J = 209.7, 11.7 Hz), 156.1, 153.9 (d, J = 7.5 Hz), 152.3, 146.2 (q, J = 5.1 Hz), 145.2, 137.2 (m), 126.9 (m), 126.6, 125.4 (q, J = 34.4 Hz), 124.1 (d, J = 23.5 Hz), 123.3, 120.2 (q, J = 271.0 Hz), 114.4 (dd, J = 16.1, 2.8 Hz), 99.6 (t, J = 27.2 Hz), 60.2, 42.7. HRAM-MS (HESI) m/z calcd for $C_{40}H_{28}F_{10}IrN_6O_4$ $[M]^+$, 1039.164; found, 1039.163.

Nuclear Magnetic Resonance. ^{1}H, ^{13}C{^{1}H}, and ^{19}F NMR spectra used for characterization were collected on a Bruker Avance NEO 400 MHz spectrometer. ^{1}H and ^{13}C NMR spectra were referenced to the relevant residual solvent peak (acetonitrile: ^{1}H δ = 1.94 ppm and ^{13}C δ = 1.32 ppm; dichloromethane: ^{1}H δ = 5.32 ppm). ^{19}F NMR spectra were referenced absolutely using the relevant residual solvent peak in the corresponding ^{1}H NMR spectrum with MestreNova software. For halide titration experiments, ^{1}H NMR spectra were collected on a Bruker Avance III 500 MHz spectrometer. A weighted-out sample of **Ir-dea** was dissolved in varying amounts of deuterated solvent to give a stock solution with a concentration of approximately 200−500 μM. 600 μL of the stock was put into a standard 5 mm NMR tube. Then a weighted-out sample of the halide salt (TBAI, TBABr, TBACl) was dissolved in varying amounts of the **Ir-dea** stock solution to obtain a concentration of approximately 2−5 mM. ^{1}H NMR spectra were collected after sequential additions of the halide containing solution via Hamilton syringe. After each addition, the NMR tube was inverted several times and vortexed for 45 s to ensure thorough mixing of the sample. The chemical resonances of protons involved in binding were tabulated as a function of halide concentration and fit to a 1:1 binding model (**Ir-dea**/halide) using the Supramolecular.org software applying the Nelder−Mead method to estimate the equilibrium constant for association.[69−71] Using the "BindSim" feature on the Supramolecular.org site, the % of iridium complexes associated was calculated using the equilibrium constant determined via ^{1}H NMR and the concentration of iridium used in each respective photoluminescence titration.

Crystallization of Ir-dea. Single crystals of **Ir-dea, Cl** were crystallized through a vapor diffusion of pentane into a concentrated DCM solution of 1:10 **Ir-dea**/TBACl. The crystallization vessel was stored at RT in a nitrogen atmosphere glovebox for 3 days to allow

https://doi.org/10.1021/acs.inorgchem.4c01726
Inorg. Chem. 2024, 63, 15772−15783

Scheme 3. Reaction Scheme for the Synthesis of Ir-dea

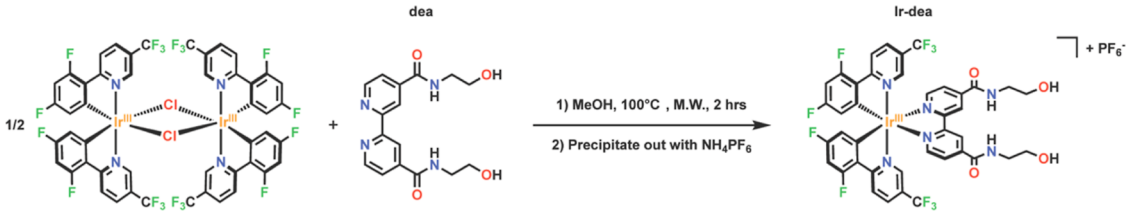

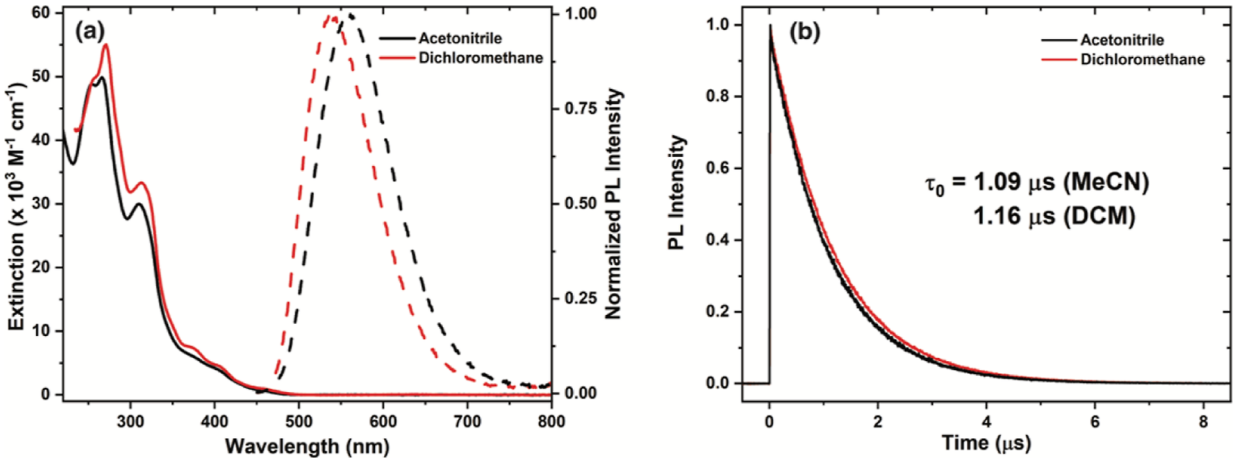

Figure 1. (a) Absorption (solid lines) and photoluminescence (dashed lines) spectra of **Ir-dea** in MeCN and DCM. (b) Time-resolved photoluminescence decay of the **Ir-dea** excited state in MeCN and DCM.

ample time for crystal growth. The Supporting Information contains relevant structural data and structure refinement.

Electrochemistry. All cyclic voltammetry experiments were performed in argon-saturated spectro-grade acetonitrile with a concentration of 0.1 M $TBAPF_6$ as the electrolyte. A three-electrode cell was utilized with a glassy carbon working electrode, Pt mesh counter electrode, and a silver wire in a $TBAPF_6$ acetonitrile solution as a pseudoreference electrode. Cyclic voltammograms were collected starting at 0 V vs the pseudo reference and scanned to negative potentials prior to positive potentials. Upon completion of data collection, a small amount of recrystallized ferrocene was added to the cell and the potential measured. All potentials were then referenced to this ferrocene/ferrocenium redox couple.[72]

Photoluminescence Sample Preparation. Samples were prepared in a dry, nitrogen atmosphere glovebox. A stock solution of the Ir photocatalyst was dissolved into acetonitrile or dichloromethane and the concentration was adjusted to an absorbance of approximately <0.1 at 420 nm (approximately <36 μM). A 3 mL aliquot of this stock was transferred to a quartz cuvette and sealed under a nitrogen atmosphere. Now to prepare the halide titrating solution, a known mass of TBAI, TBABr, or TBACl was dissolved in the Ir stock solution to keep [Ir] constant throughout the titration experiment. Titration additions to the cuvette were performed using Hamilton syringes in a glovebox atmosphere.

UV−Vis Absorption. Absorption spectra were collected using an Agilent Cary 60 UV−Vis spectrophotometer from 200 to 800 nm with a scan rate of 1200 nm/min. Extinction coefficients were determined from the titration of an **Ir-dea** solution of a known concentration into a known volume of neat solvent. A linear fit of concentration dependent absorbance spectra provided the desired extinction coefficient.

Nanosecond Time-Resolved Photoluminescence. Nanosecond time-resolved photoluminescence decays were collected using a Photon Technology International (PTI) GL-301 nitrogen dye laser with a 440 nm excitation. The PL was detected by a Hamamatsu R928 PMT optically coupled to a ScienceTech model 9010 monochromator terminated into a LeCroy Waverunner LT322 oscilloscope. Radiative and nonradiative rates for photoluminescence decay were calculated from the quantum yields and the excited-state lifetime in the absence of quencher using the following equations; $\phi_{PL} = k_r/(k_r + k_{nr})$, $\tau = 1/(k_r + k_{nr})$.[73]

Steady-State Photoluminescence. All steady-state PL spectra were recorded using a Horiba Fluorolog 3 fluorimeter equipped with a standard xenon lamp. All samples were excited with 420 nm light and monitored from 450 to 800 nm. The intensity was integrated for 0.1 s at 2 nm resolution and averaged over three scans. Quantum yields for photoluminescence were measured via comparative actinometry using Coumarin 500 (ϕ_{PL} = 0.681) in methanol as a standard.[73,74] The quantum yields of the halide adducts were measured after the addition of 1 mol equiv of the tetrabutylammonium halide salt.

RESULTS

The **Ir-dea** photocatalyst was synthesized according to Scheme 3. The synthesis of the **dea** ligand has been reported previously and was reacted with a commercially available iridium bridged chloride dimer to yield the desired photocatalyst.[68]

Ir-dea was characterized via ^1H, ^{13}C, and ^{19}F NMR spectroscopy in d_3-MeCN (Figures S1−S3). UV−visible spectroscopy indicates intense ligand-centered absorptions in the near-UV region and a much weaker absorption in the blue region assigned to a metal-to-ligand charge-transfer (MLCT), Figure 1a. Upon 420 nm excitation, a broad photoluminescence centered around 560 nm (acetonitrile) and 539 nm (dichloromethane) was observed.

The excited state lifetime, τ_0, was determined after pulsed 440 nm laser excitation, yielding lifetimes of τ_0 = 1.09 μs (acetonitrile) and τ_0 = 1.16 μs (dichloromethane) (Figure 1b). Cyclic voltammetry experiments of **Ir-dea** indicated a quasi-reversible $E^{\circ\prime}$ ($Ir^{+/0}$) of −1.38 V vs $Fc^{+/0}$ in acetonitrile and −1.35 V vs $Fc^{+/0}$ in dichloromethane with 0.1 M $TBAPF_6$ as the supporting electrolyte (Figures S4 and S5). The wave was assigned as quasi-reversible due to a peak splitting that was larger than 59 mV (MeCN: ∼73 mV, Fc/Fc^+ peak splitting was

https://doi.org/10.1021/acs.inorgchem.4c01726
Inorg. Chem. 2024, 63, 15772−15783

86 mV; DCM: ~83 mV, Fc/Fc^+ peak splitting was 202 mV) and deviations between the integrated oxidative and

$$E^{\circ\prime}(Ir^{*+/0}) = E^{\circ\prime}(Ir^{+/0}) + \Delta G_{ES} \quad (1)$$

reductive current.[75] The free energy stored in the excited state, ΔG_{ES}, was estimated from a tangent line of the blue edge of the PL spectrum (ΔG_{ES} = 2.55 eV in MeCN and 2.60 eV in DCM). The oxidizing power of the excited state was determined in both solvents using eq 1 (Table 1).[76]

Table 1. Relevant Photophysical Data of Ir-dea in Both Acetonitrile and Dichloromethane

	τ_0 (ns)	ΔG_{ES} (eV)	PL_{max} (nm)	$E^{\circ\prime}$ ($Ir^{+/0}$) (V vs $Fc^{+/0}$)	$E^{\circ\prime}$ ($Ir^{*+/0}$) (V vs $Fc^{+/0}$)
MeCN	1090	2.55	560	−1.38	1.17
DCM	1160	2.60	539	−1.35	1.25

Equilibrium constants for halide association with **Ir-dea** were determined through titration experiments with a ^1H NMR assay. This analysis also provided the preferred location of halide association as several of the resonances shifted upon titration while others remained unchanged. As a representative example, the addition of tetrabutylammonium chloride induced a substantial downfield shift of the 3,3′ bipyridine protons (labeled "e"), the amide protons (labeled "d"), and the alcohol protons (labeled "a") until the addition of 1 equiv of the chloride salt upon which shifting ceased, Figure 2.

The titration data for tetrabutylammonium bromide and iodide in d_3-MeCN also revealed similar shifts in the noted resonances. However, the spectral changes induced by bromide and iodide did not cease until 4 and >9 equiv, respectively (Figures S6 and S7).

In d_2-DCM, the same key resonances shifted downfield upon halide addition, yet ceased at 1 equiv for all the halide ions in this solvent (Figures S8−S10). These titrations indicate that the halide was localized within the designed hydrogen bonding "pocket" of the **dea** ligand. Small shifts in other peaks, such as the ethylene spacer (labeled "b" and "c") between the amide and alcohol protons and the 5,5′ bipyridine protons on the **dea** ligand were also observed but were much less dramatic than for those H atoms directly involved in hydrogen bonding.

The shifts in resonances associated with hydrogen bonding were fit to a 1:1 binding model to extract the desired equilibrium constants for halide association and are reported in Table 2.[69−71] This stoichiometry was chosen as only one halide was anticipated to associate based on the ligand structure and monocationic nature of the complex. This stoichiometry was also confirmed via X-ray crystallography described *vide infra*. Over the concentration range studied, the amide proton (−NH) resonances were impacted the most. This was the case for every halide in both solvents except for chloride in d_2-DCM,

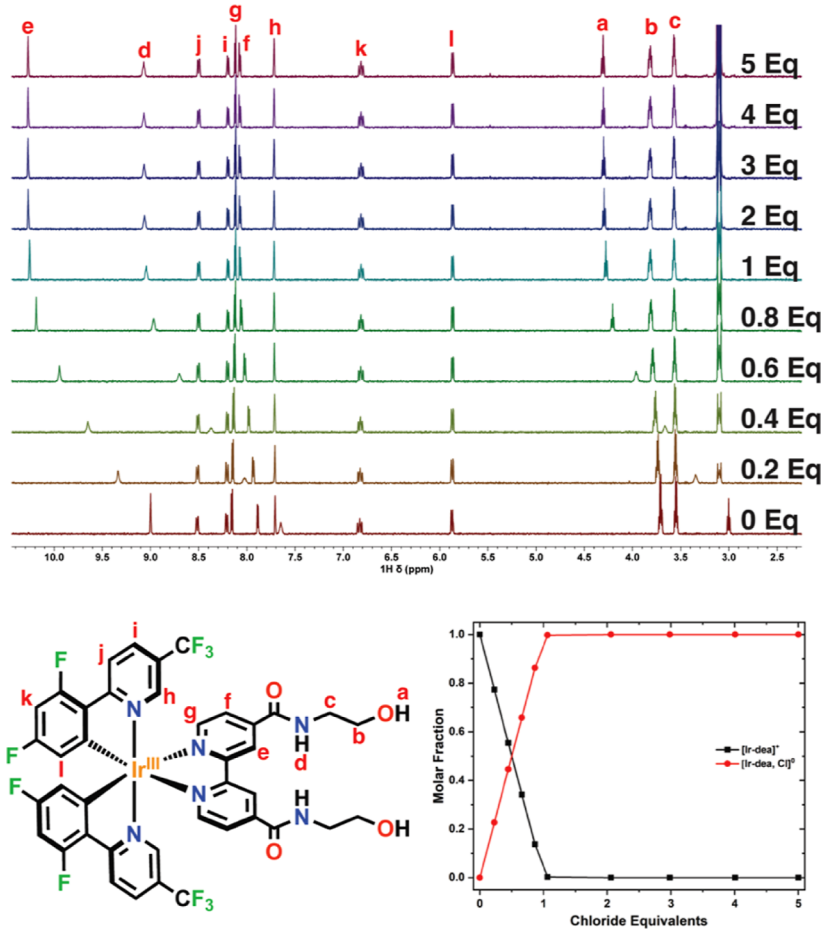

Figure 2. ^1H NMR titration of **Ir-dea** with TBACl in d_3-MeCN and the molar fraction plot showing the ratio between the parent complex and the halide adduct as a function of chloride equivalents. NMR titration measurements were performed at an **Ir-dea** concentration of ~380 μM in the designated deuterated solvent.

https://doi.org/10.1021/acs.inorgchem.4c01726
Inorg. Chem. 2024, 63, 15772−15783

Table 2. Equilibrium Constants for Halide Association with Ir-dea and the Observed Change in Chemical Shift of the Hydrogen Bonding Protons in Both Acetonitrile and Dichloromethane

		Δppm		
	K_{eq} (M^{-1})	3,3′ H	−NH	−OH
		MeCN		
I^-	1.3×10^3	0.57	0.77	0.21
Br^-	8.8×10^4	1.14	1.34	0.70
Cl^-	$>10^6$	1.27	1.42	1.31
		DCM		
I^-	$>10^6$	1.17	1.38	0.68
Br^-	$>10^6$	1.39	1.47	1.28
Cl^-	$>10^6$	1.49	1.52	1.90

where the −OH resonances shifted 1.90 ppm. The magnitude of the peak shift, Δppm, trended with the ionic radius of the halides, where chloride showed the largest shifts and iodide showed the smallest. In d_3-MeCN, I^- showed the smallest equilibrium constant at $K_{eq} = 1.3 \times 10^3$ M^{-1} and increased by an order of magnitude to $K_{eq} = 8.8 \times 10^4$ M^{-1} for Br^- and a lower limit of $K_{eq} > 10^6$ M^{-1} for Cl^-. In the less polar d_2-DCM, the equilibrium constants for halide association increased to greater than 10^6 M^{-1}. The equilibrium constants in acetonitrile indicate that this complex has selectivity for binding chloride over bromide and iodide.

Titrations of the tetrabutylammonium halide salts also resulted in a blue shift of the PL maximum whose magnitude was both solvent and halide dependent. In acetonitrile, a blue shift of 7−15 nm (28−53 eV) was observed increasing from iodide to chloride. In dichloromethane, a blue shift of 25 nm (112 eV) was observed for all three halides.

Acetonitrile. Excited state quenching experiments revealed a decrease in the steady state photoluminescence intensity and the excited state lifetime as a function of the iodide concentration. Through a Stern−Volmer (SV) analysis of the lifetimes (τ_0/τ), a first-order dependence on iodide concentration was evident, indicative of a dynamic quenching mechanism.[77] In addition, a small decrease in the initial amplitude of the time-resolved photoluminescence decay was observed, indicative of static quenching (Figure 3b, inset). This amplitude decrease is attributed to the formation of a nonluminescent adduct between the photocatalyst and halide via the static quenching pathway.[77−79] A Stern−Volmer (SV) analysis of the steady-state photoluminescence (I_0/I) yielded

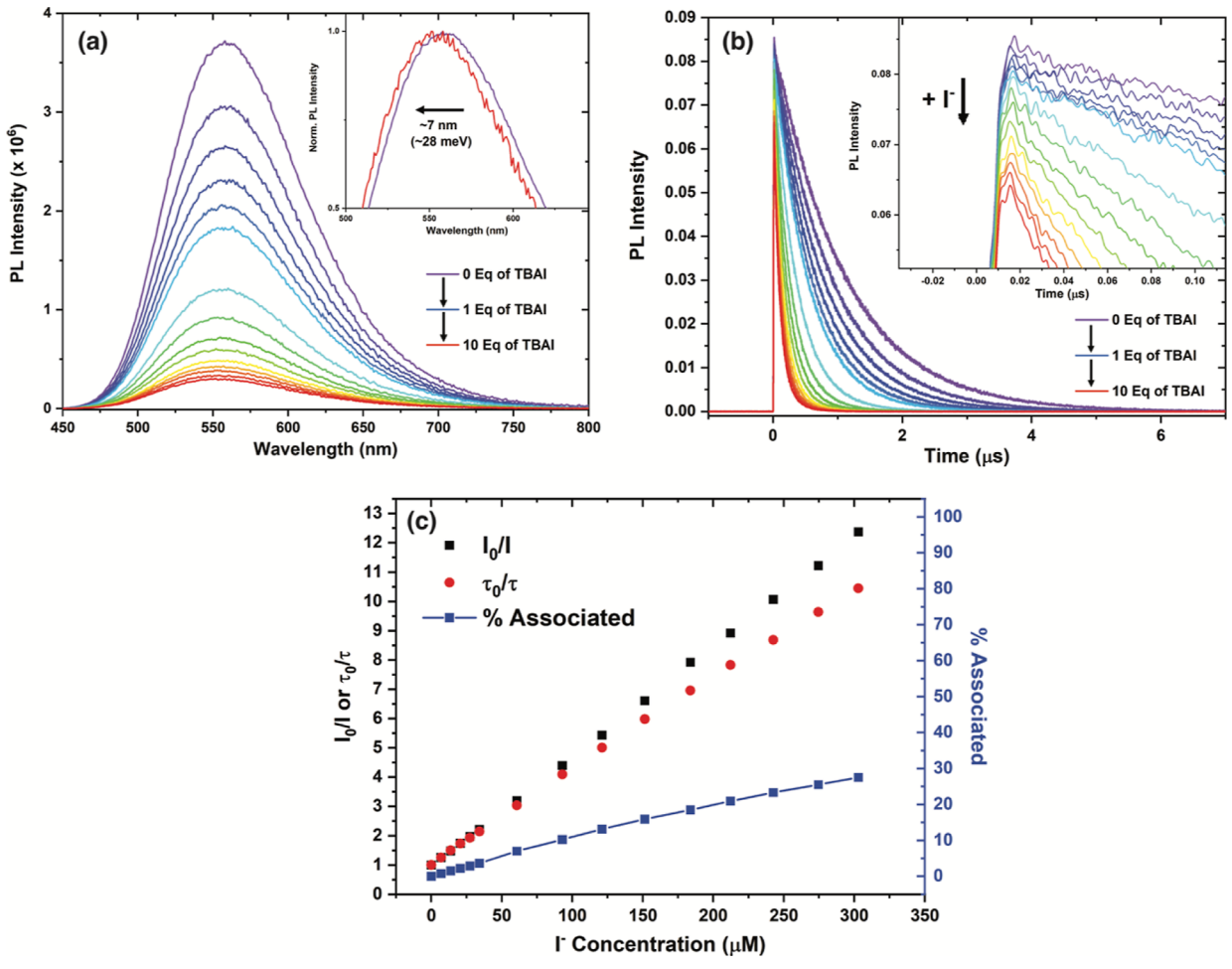

Figure 3. (a) Steady-state photoluminescence quenching of **Ir-dea** by iodide in MeCN (inset: normalized SS PL showing the blue shift in the λ_{em} maximum). (b) Time-resolved photoluminescence quenching of **Ir-dea** by iodide in MeCN (inset: a zoom of the first 100 ns, showing the decrease in initial amplitude with the addition of iodide). (c) Stern−Volmer plot of the SS and TR PL as a function of total [I^-] and the % of iridium complexes associated as a function of total [I^-] on the right y-axis. PL measurements were performed at an **Ir-dea** concentration of ∼30 μM in each respective solvent.

https://doi.org/10.1021/acs.inorgchem.4c01726
Inorg. Chem. 2024, 63, 15772−15783

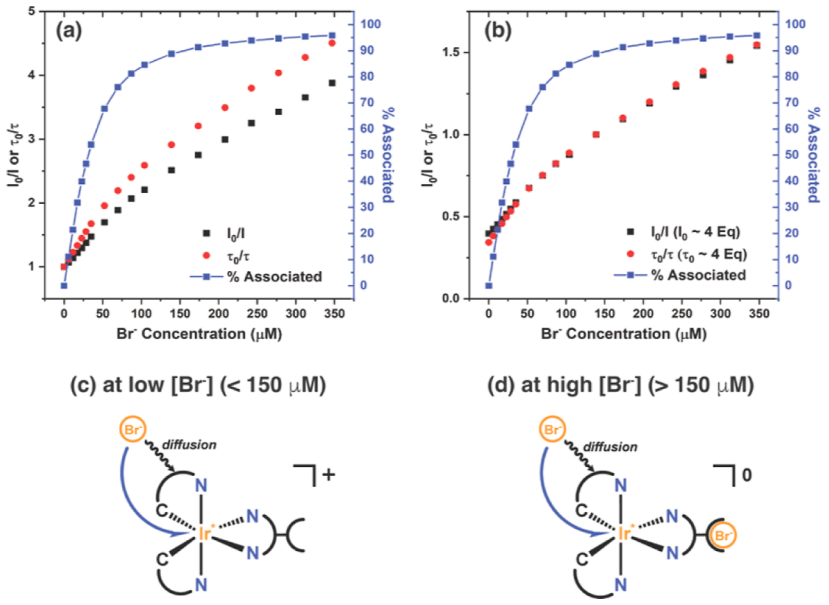

Figure 4. (a) Stern–Volmer plot of the I_0/I and τ_0/τ as a function of total [Br^-] treating I_0 and τ_0 as 0 equiv of added bromide and the % of iridium complexes associated as a function of total [Br^-] on the right *y*-axis. (b) Stern–Volmer plot of the same data as in (a) with I_0 and τ_0 as the PL intensity and lifetime measured with 4 equiv of bromide. (c) Simplistic structure showing the monocationic parent complex quenching bromide dynamically which primarily occurs at low bromide concentrations (<150 μM). (d) Simplistic structure showing the neutral bromide adduct quenching dynamically which primarily occurs at high bromide concentrations (>150 μM). PL measurements were performed at an **Ir-dea** concentration of ~30 μM in each respective solvent.

an upward curving plot at high iodide concentrations, data consistent with both the static and dynamic quenching mechanisms (Figure 3c).[77−79] Also included in Figure 3c is the percentage of the iridium complexes which are associated with an iodide ion (% associated).

Bromide quenched both the steady-state photoluminescence intensity and the excited state lifetime (Figure S11). A Stern–Volmer analysis of both I_0/I and τ_0/τ revealed a decline in the overall quenching efficiency upon sequential additions of TBABr (Figure 4a). Two regimes with unique quenching rate constants were observed in the SV plots. Interestingly, the plots of I_0/I and τ_0/τ differed considerably. However, much better agreement was evident when the I_0 and τ_0 were assigned to the values measured with 4 equiv of bromide and deviation was limited to the low bromide concentration regime (Figure 4b). Note that when the same experiment was performed in 0.1 M $TBAPF_6$ electrolyte solutions both the steady-state and lifetime SV plots displayed the expected linear behavior, indicative that this decline in quenching is due to the association of bromide with **Ir-dea** (Figure S12).

Titration with TBACl showed behavior anomalous to the other halides and were consistent with a previous report of a related ruthenium photocatalyst.[68] Most notably, the addition of 1 equivalent of chloride increased the quantum yield for photoluminescence (ϕ_{PL}) from 0.48 to 0.55 and yielded an ~15 nm (~53 meV) blue shift of the photoluminescence spectrum (Figure 4a). The excited state lifetime also increased with one equivalent of chloride from τ_0 = 1.09 to 1.12 μs (Figure S13). The lifetimes and quantum yields were used to determine the radiative (k_r) and nonradiative (k_{nr}) rate constants before and after the formation of the chloride adduct, eqs 2 and 3 (Table 3). An increase in k_r and a decrease in k_{nr} were observed with the formation of the chloride adduct.

$$\phi_{PL} = k_r/(k_r + k_{nr}) \quad (2)$$

$$\tau_0 = 1/(k_r + k_{nr}) \quad (3)$$

Table 3. Excited State Lifetime (τ), Photoluminescence Quantum Yield, (ϕ_{PL}), and the Radiative (k_r) and Nonradiative (k_{nr}) Rate Constants for Ir-dea* in Acetonitrile and Dichloromethane

	τ (ns)	ϕ_{PL}	k_r ($\times 10^5$ s^{-1})	k_{nr} ($\times 10^5$ s^{-1})
		MeCN		
Ir-dea, PF_6	1090	0.48	4.3	4.7
Ir-dea, Cl[a]	1120	0.55	5.0	4.1
		DCM		
Ir-dea, PF_6	1160	0.70	6.0	2.5
Ir-dea, Br[a]	980	0.73[b]	7.6	2.8[b]
Ir-dea, Cl[a]	1060	0.82	7.6	1.6

[a]One equiv of bromide and chloride were present. [b]Some static quenching is hypothesized to occur and as such the measured relative quantum yield includes competitive nonradiative electron transfer.

Further addition of chloride beyond one equivalent yielded dynamic quenching of the freely diffusing chloride by the photoexcited **Ir-dea, Cl** adduct. A Stern–Volmer analysis of the steady-state photoluminescence and the excited state lifetime is shown in Figure 5c.

Dichloromethane. Titration of TBAI in DCM results in an immense loss in the steady-state PL intensity up to 1 equiv of added iodide yielding an I_0/I value of 20.2. At higher equivalents, the steady state PL intensity decreased slightly to a value of 19.6 (Figure S14). Similarly, the time-resolved PL data revealed lifetime quenching and an immense loss in the initial amplitude until 1 equiv of iodide (Figure 6a). Further addition of iodide past 1 equiv, led to an increase in the initial amplitude of the time-resolved photoluminescence and a further decrease in the excited state lifetime. A control experiment was performed where 1 equiv of TBAI was titrated

https://doi.org/10.1021/acs.inorgchem.4c01726
Inorg. Chem. 2024, 63, 15772−15783

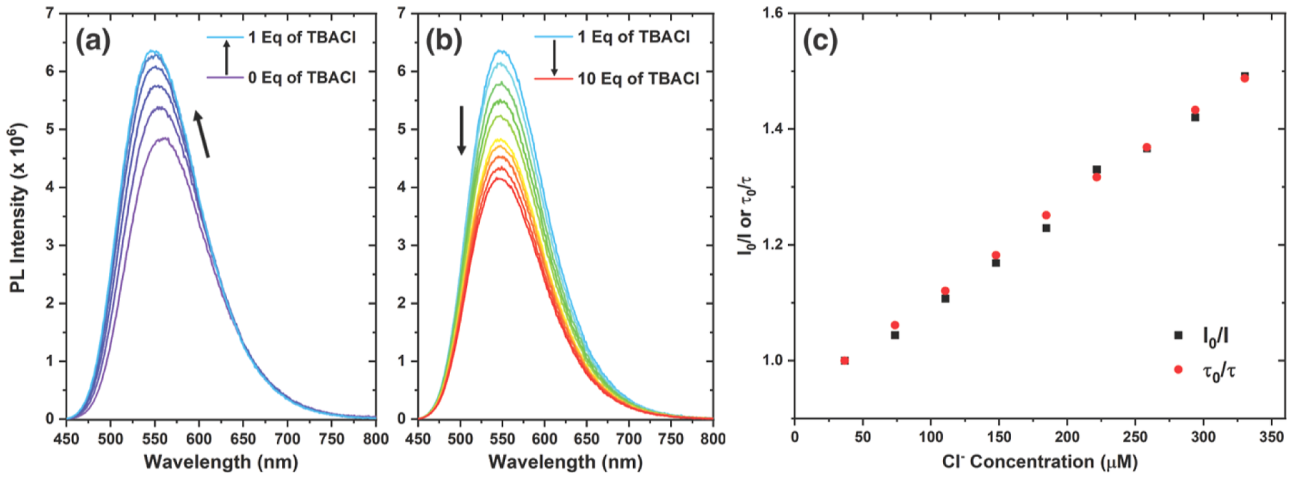

Figure 5. (a) Steady-state photoluminescence intensity increase and blue shift with the addition of 1 equiv of TBACl to **Ir-dea** in MeCN. (b) The steady-state photoluminescence quenching of **Ir-dea, Cl** by TBACl in MeCN. (c) Stern–Volmer plot of the steady-state and lifetime quenching of **Ir-dea, Cl** by TBACl in MeCN. PL measurements were performed at an **Ir-dea** concentration of ∼30 μM in each respective solvent.

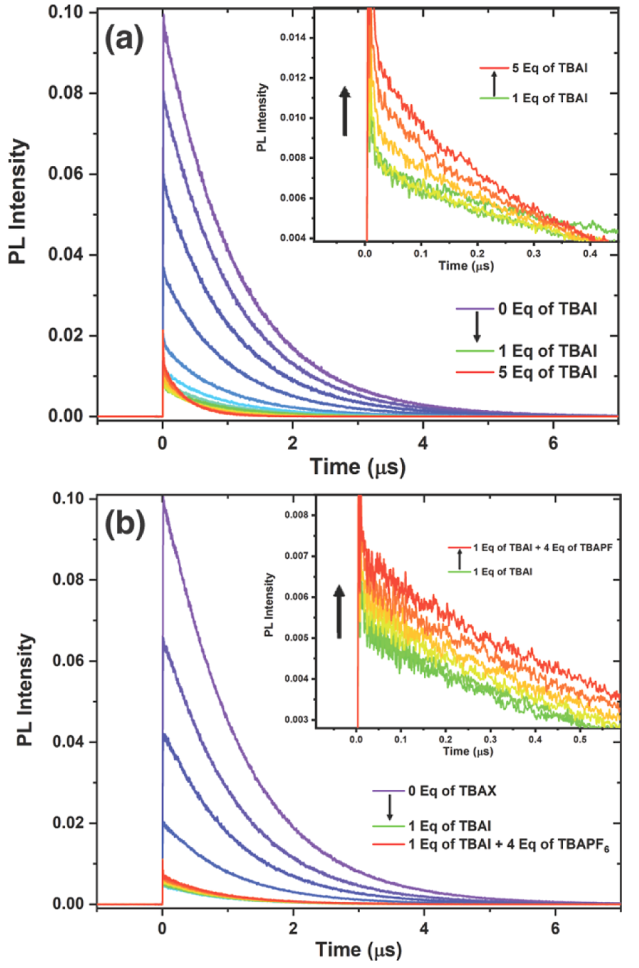

Figure 6. (a) Time-resolved photoluminescence measured after pulsed 440 nm excitation of **Ir-dea** in the presence of iodide in DCM (inset: zoom in of the increase in initial amplitude with added iodide). (b) Time-resolved photoluminescence quenching of **Ir-dea** by 1 equiv of iodide followed by additions of $TBAPF_6$ (inset: zoom in of the increase in initial amplitude with added $TBAPF_6$). PL measurements were performed at an **Ir-dea** concentration of ∼30 μM.

into a solution of **Ir-dea** followed by sequential additions of $TBAPF_6$ (Figure S15). The addition of 1 equiv of iodide decreased the PL intensity and lifetime with a significant decrease in the initial amplitude of the TR PL. The subsequent addition of $TBAPF_6$ resulted in an increase in SS PL and the initial amplitude with no further quenching of the lifetime. It is also worth noting that in both the iodide titration and the control, a short lifetime of <10 ns, that was within the instrument response time of our apparatus, was observed upon iodide addition.

A SV analysis of the time-resolved photoluminescence data was linearly dependent on halide concentration indicative of dynamic quenching. The steady-state SV analysis showed immense upward curvature until the addition of 1 equiv upon which the plot began to decrease slightly (Figure S14). The control experiment yielded a similar SV plot from 0 to 1 equiv of added iodide but decreased more significantly in the I_0/I plot and decreased slightly in the τ_0/τ plot with the addition of $TBAPF_6$.

Interestingly, in DCM, both bromide and chloride adduct initially increased the photoluminescence quantum yield while the excited state lifetime decreased by 180 ns for bromide and 100 ns for chloride (Figures S16 and S18). Use of eqs 2 and 3 revealed that k_r increased significantly for both while k_{nr} increased for bromide and decreased for chloride. It is also of import to note that the initial amplitude of the time-resolved photoluminescence decreased with 1 equiv of bromide addition but did not for chloride. Upon further additions after 1 equiv, the steady state PL and excited state lifetime of the bromide and chloride adducts were dynamically quenched by freely diffusing bromide and chloride respectively, as evident by a linear Stern–Volmer plot (Figures S17 and S19).

DISCUSSION

The iridium photocatalyst (**Ir-dea**) is shown to be competent for associating a halide ion with the pendant hydrogen-bonding amide and alcohol groups. This ground state "preassociation" gave rise to the possibility of a rapid intra-ionic excited state electron transfer reaction (static quenching) as well as diffusional (dynamic quenching) reactions wherein the excited photocatalyst and quencher transfer electrons within encounter complexes formed by diffusional interactions.[77,78,80] The data

https://doi.org/10.1021/acs.inorgchem.4c01726
Inorg. Chem. 2024, 63, 15772−15783

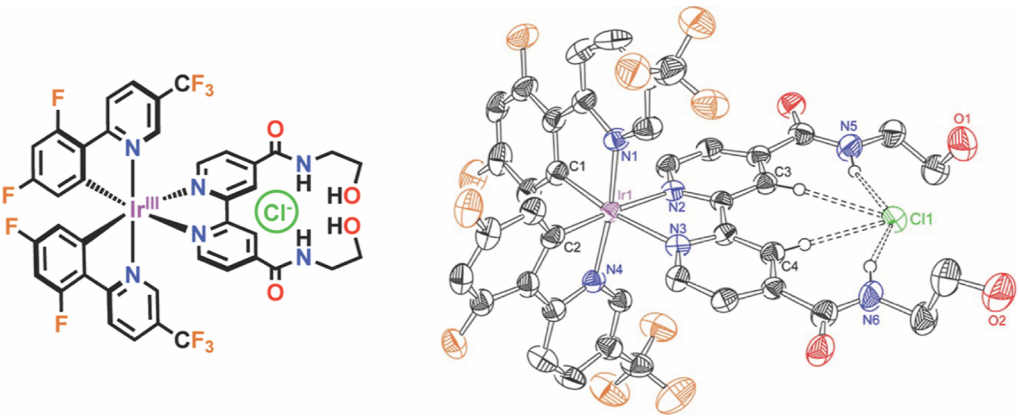

Figure 7. Solid-state structure of **Ir-dea, Cl** as determined via X-ray crystallography with thermal ellipsoids at 50%. Solvent molecules and noninteracting H atoms omitted for clarity. The N5, N6, C3, C4 hydrogen atoms form a "binding pocket" for a halide to associate.

reported herein reveal that the excited state quenching pathway(s) is sensitive to the identity of the halide ion and to the nature of the solvent. Below we first discuss the proposed structure and thermodynamic properties of the ground state adducts followed by the excited state reactivity, all through the lens of periodic trends.

Determination of Halide Binding Affinity and Location. ^{1}H NMR spectroscopy was utilized as a powerful tool to quantify the equilibrium constants for halide association and the physical location of the H-bonding interactions. Halide titration studies revealed dramatic downfield shifts in the ^{1}H resonances assigned to the 3,3′-bipyridine, amide, and alcohol hydrogens while other resonances were largely unaffected. The downfield direction of these shifts is consistent with a hydrogen bonding interaction with the halide that induces a decrease in the electron density of the H atom, deshielding the nucleus from the magnetic field. Peak broadening and the observation of a single resonance when substoichiometric amounts of the halide were present indicated that halide exchange is fast on the ^{1}H NMR time scale.[68,78,80−83]

Equilibrium constants, K_{eq}, measured in d_3-MeCN increased in the order $I^- < Br^- < Cl^-$ and varied over three-order of magnitude from 10^3 (I^-) and $>10^6$ M^{-1} (Cl^-). This periodic trend has been previously reported in the anion recognition literature and attributed to the size-to-charge ratio of these ions.[60,61,63,68,84] In dichloromethane, the K_{eq} values for all three halides were too large to be accurately determined by ^{1}H NMR, behavior consistent with the lower dielectric constant of DCM (ε = 8.93) relative to MeCN (ε = 37.5).[68,85]

Importantly, the symmetry of the photocatalyst is maintained throughout the titration indicating that the halide associates along the C_2 axis that defines the **dea** ligand. For chloride, this location was also present in the solid state, as shown by X-ray crystallographic data (Figures 7 and S20). The solid state structure reported herein is consistent with previously reported X-ray crystallographic data of structurally similar hydrogen bonding halide adducts.[55,84,86−89] The X−H···Cl^- (X = C, N) interatomic distances of the **Ir-dea, Cl** crystal structure agreed well with other reported crystal structures of halide adducts with pendant amides on bipyridine ligands (Table S1). Additionally, a planarization of the amide groups with the bipyridine moiety was observed in agreement with literature observation (Figures S21).[68]

It is interesting to note however that the −OH groups did not substantially interact with the chloride anion in the solid-state yet in d_3-MeCN or d_2-DCM solutions the associated resonances displayed large downfield shifts. In the solid state, the −OH substituents were hydrogen bonding with another **Ir-dea, Cl** molecule in the crystal lattice (Figure S22). However, as discussed above, ^{1}H NMR spectra measured of **Ir-dea, Cl** suggest a meaningful interaction in homogeneous solution.

Excited State Quenching Studies. Intra-ionic excited state electron transfer was possible for the halide present in the "binding pocket". However, iodide was the only ion with evidence for intra-ionic electron transfer while there was no evidence by associated chloride. Bromide showed intermediate behavior where intra-ionic electron transfer was only evident in dichloromethane. This trend is expected based on the gas phase electron affinities given in Scheme 1, the $E^{\circ\prime}$ ($X^{\bullet/-}$) reduction potentials, and the equilibrium constants for halide association.[1] The H-bonding interactions with the **dea** ligand modulate the one-electron halide reduction potentials. With the measured equilibrium constants as a crude indicator of the extent of halide stabilization, the shift in the reduction potentials upon association would be largest for chloride and smallest for iodide.[80]

The excited state reduction potential of the Ir photocatalyst is $E^{\circ\prime}$ ($Ir^{*+/0}$) = +1.17 V vs $Fc^{+/0}$ in MeCN. The halogen reduction potentials in organic solvents are generally unknown and require nontrivial kinetic and/or computational determination.[35,42−47,78] However, the most reliable values are for iodide in MeCN solutions due to its wide-use in dye-sensitized solar cells, $E^{\circ\prime}$ ($I^{\bullet/-}$) = 0.7 V vs $Fc^{+/0}$.[1,90,91] If one assumes that all of the stabilization associated with adduct formation is

$$\Delta G^{\circ}_{eq} = -RT\ln(K_{eq}) \quad (4)$$

attributed to the iodide anion, the driving force for stabilization can be estimated from the equilibrium constant to be 180 meV, calculated from eq 4. Hence, the driving force for static iodide oxidation would be −290 meV, consistent with the rapid intra-ionic quenching. We note that assigning all of the free energy of association to the iodide ion is an extreme that represents that maximum shift in the halogen reduction potential. While this assumption has been previously used in the literature where electrostatics are expected to be the predominant noncovalent interaction, a recent study shows that stabilization of the halogen atom product is also important when estimating ΔE° ($X^{\bullet/-}$).[78,80]

Bromide yielded behavior intermediate of that observed for iodide and chloride. In acetonitrile, the Stern−Volmer plot

https://doi.org/10.1021/acs.inorgchem.4c01726
Inorg. Chem. 2024, 63, 15772−15783

revealed two linear regimes for bromide quenching. Previous reports concluded that these regimes arise from a change in the effective charge of the photocatalyst that in turn, impacts the diffusional rate constants.[1,82] Thus, at low bromide concentrations, the [**Ir-dea**]$^{*+}$ monocationic photocatalyst was quenched primarily while at high concentrations, the neutral [**Ir-dea**, Br^-]^{*0} was quenched (Figure 4c,d). The two regimes were not present in a high ionic strength environment, further evidence that the association induced the change in the diffusion rate constant.

The diffusional quenching rate constants followed the periodic trends expected for the halides. In DCM, a halide associated stoichiometrically with the photosensitizer and quenching of the adduct by a free halide was quantified. The diffusional quenching rate constants increased when going down the periodic column, consistent with the gas phase electron affinities, estimated one-electron reduction potentials of the halides, and other reports of halide quenching.[1,35,68,78,92,93] Iodide was quenched with a rate constant 1.5×10^{10} M^{-1} s^{-1} which decreased to 7.9×10^{9} M^{-1} s^{-1} for bromide and 2.5×10^{9} M^{-1} s^{-1} for chloride.

Finally, we note that halide association had a measurable impact on the free energy stored in the excited state. The halides induced an increase in the ground-excited state energy gap as evidenced by a blue shift in the PL spectra. Interestingly a periodic trend was observed in acetonitrile while in dichloromethane a large shift of 112 meV was observed that was independent of the halide ion. The increased energy gap can be understood as a destabilization of the π^* levels of the **dea** ligand induced by the halide interacting with the MLCT excited state.

On the basis of the energy gap law, a blue shift is expected to result in an increase excited state lifetime through a decrease in the nonradiative rate constant (k_{nr}).[94] Such behavior was most easily characterized for chloride where intra-ionic quenching was absent. In MeCN, the expected increase in the excited state lifetime and decreased k_{nr} were observed. Surprisingly a decrease in the excited state lifetime was measured in DCM due to a substantial increase in the radiative rate constant (k_r). The increase in k_r was also observed for both bromide and chloride in DCM and is in qualitative agreement with Fermi's Golden Rule.[95−97] Interestingly, 1 equiv of bromide induced an increase in k_{nr}, in contradiction to the time-honored energy gap law.[94] This is hypothesized as a small amount of static quenching, as evidenced by a decrease in the initial amplitude of the time-resolved photoluminescence. As electron transfer is a nonradiative decay pathway for the excited state, this would yield an increase in k_{nr}.

CONCLUSIONS

A novel Ir(III) photocatalyst was synthesized and used to sensitize iodide, bromide and chloride primarily through hydrogen bonding stabilization by an amide moiety. The binding affinity for halide association was highly dependent on the atomic radius of the halide as well as the polarity of the solution medium. Being able to tune binding selectivity for anions of like charge is of key importance to the anion recognition community and to those looking to selectively sequester anions from complex mixtures such as chloride in seawater.

After blue light excitation of the halide adducts, two electron transfer mechanisms (intra-ionic and diffusional) can arise competitive with excited state decay. The prominence of each mechanism was dependent on the binding affinity of the halide, the electron affinity of the halide, and the driving force for photo-oxidation. Photo-oxidation of each solvated halide was achieved through the dynamic quenching mechanism. However, intra-ionic quenching was more scarce due to the stabilization imposed on the halides making intra-ionic photo-oxidation thermodynamically arduous. These studies provide valuable insight into the impact of noncovalent interactions on the photophysics and intra-ionic photo-oxidation of halide adducts as well as assist in the design of more efficient and suitable photoredox systems or anion sensors.

ASSOCIATED CONTENT

Supporting Information

The Supporting Information is available free of charge at https://pubs.acs.org/doi/10.1021/acs.inorgchem.4c01726.

^{1}H, ^{13}C, and ^{19}F NMR characterization of **Ir-dea**; cyclic voltammetry; ^{1}H NMR titrations and molefraction plots; photoluminescence titrations and Stern−Volmer analysis; and X-ray crystallography data are available (PDF)

Accession Codes

CCDC 2350922 contains the supplementary crystallographic data for this paper. These data can be obtained free of charge via www.ccdc.cam.ac.uk/data_request/cif, or by emailing data_request@ccdc.cam.ac.uk, or by contacting The Cambridge Crystallographic Data Centre, 12 Union Road, Cambridge CB2 1EZ, UK; fax: +44 1223 336033.

AUTHOR INFORMATION

Corresponding Author

Gerald J. Meyer − *Department of Chemistry, University of North Carolina at Chapel Hill, Chapel Hill, North Carolina 27599, United States;* orcid.org/0000-0002-4227-6393; Email: gjmeyer@email.unc.edu

Authors

Matthew J. Goodwin − *Department of Chemistry, University of North Carolina at Chapel Hill, Chapel Hill, North Carolina 27599, United States;* orcid.org/0000-0002-4790-3501

Alexander M. Deetz − *Department of Chemistry, University of North Carolina at Chapel Hill, Chapel Hill, North Carolina 27599, United States;* orcid.org/0000-0003-4324-0584

Paul J. Griffin − *Department of Chemistry, University of North Carolina at Chapel Hill, Chapel Hill, North Carolina 27599, United States;* orcid.org/0000-0001-5482-3457

Complete contact information is available at: https://pubs.acs.org/10.1021/acs.inorgchem.4c01726

Notes

The authors declare no competing financial interest.

ACKNOWLEDGMENTS

The research was supported by the National Science Foundation under Award CHE-2247589. We would like to thank John Dickenson for collection of HRMS data of **Ir-dea** and for useful discussions. We would also like to thank Dr. Chun-Hsing Chen for assisting with collection and analysis of X-ray crystallography data. The X-ray crystallography work is supported by the National Science Foundation under grant no. CHE-2117287.

REFERENCES

(1) Troian-Gautier, L.; Turlington, M. D.; Wehlin, S. A. M.; Maurer, A. B.; Brady, M. D.; Swords, W. B.; Meyer, G. J. Halide Photoredox Chemistry. *Chem. Rev.* **2019**, *119* (7), 4628−4683.

(2) Popov, A. I. *Halogen Chemistry*; Gutmann, V., Ed.; Academic Press: London, NY, 1967.

(3) Busch, M. A. Halogen Chemistry. In *Encyclopedia of Physical Science and Technology*, 3rd ed.; Meyers, R. A., Ed.; Academic Press, 2003; pp 197−222.

(4) Kim, J. Y.; Lee, J. W.; Jung, H. S.; Shin, H.; Park, N. G. High-Efficiency Perovskite Solar Cells. *Chem. Rev.* **2020**, *120* (15), 7867−7918.

(5) Jošt, M.; Kegelmann, L.; Korte, L.; Albrecht, S. Monolithic Perovskite Tandem Solar Cells: A Review of the Present Status and Advanced Characterization Methods Toward 30% Efficiency. *Adv. Energy Mater.* **2020**, *10*, 1904102.

(6) Peter, L. Sticky electrons transport and interfacial transfer of electrons in the dye-sensitized solar cell. *Acc. Chem. Res.* **2009**, *42* (11), 1839−1847.

(7) Gong, J.; Sumathy, K.; Qiao, Q.; Zhou, Z. Review on dye-sensitized solar cells (DSSCs): Advanced techniques and research trends. *Renew. Sustain. Energy Rev.* **2017**, *68*, 234−246.

(8) Hagfeldt, A.; Boschloo, G.; Sun, L.; Kloo, L.; Pettersson, H. Dye-sensitized solar cells. *Chem. Rev.* **2010**, *110* (11), 6595−6663.

(9) McDaniel, N. D.; Bernhard, S. Solar fuels: thermodynamics, candidates, tactics, and figures of merit. *Dalton Trans.* **2010**, *39* (42), 10021−10030.

(10) Powers, D. C.; Hwang, S. J.; Zheng, S. L.; Nocera, D. G. Halide-bridged binuclear HX-splitting catalysts. *Inorg. Chem.* **2014**, *53* (17), 9122−9128.

(11) Powers, D. C.; Anderson, B. L.; Nocera, D. G. Two-electron HCl to H2 photocycle promoted by Ni(II) polypyridyl halide complexes. *J. Am. Chem. Soc.* **2013**, *135* (50), 18876−18883.

(12) Heyduk, A. F.; Nocera, D. G. Hydrogen produced from hydrohalic acid solutions by a two-electron mixed-valence photocatalyst. *Science* **2001**, *293* (5535), 1639−1641.

(13) Hwang, S. J.; Powers, D. C.; Maher, A. G.; Anderson, B. L.; Hadt, R. G.; Zheng, S. L.; Chen, Y. S.; Nocera, D. G. Trap-Free Halogen Photoelimination from Mononuclear Ni(III) Complexes. *J. Am. Chem. Soc.* **2015**, *137* (20), 6472−6475.

(14) Shaw, M. H.; Twilton, J.; MacMillan, D. W. Photoredox Catalysis in Organic Chemistry. *J. Org. Chem.* **2016**, *81* (16), 6898−6926.

(15) Romero, N. A.; Nicewicz, D. A. Organic photoredox catalysis. *Chem. Rev.* **2016**, *116* (17), 10075−10166.

(16) Wang, C. S.; Dixneuf, P. H.; Soule, J. F. Photoredox Catalysis for Building C-C Bonds from C(sp(2))-H Bonds. *Chem. Rev.* **2018**, *118* (16), 7532−7585.

(17) Narayanam, J. M.; Stephenson, C. R. Visible light photoredox catalysis: applications in organic synthesis. *Chem. Soc. Rev.* **2011**, *40* (1), 102−113.

(18) Li, P.; Deetz, A. M.; Hu, J.; Meyer, G. J.; Hu, K. Chloride Oxidation by One- or Two-Photon Excitation of N-Phenylphenothiazine. *J. Am. Chem. Soc.* **2022**, *144* (38), 17604−17610.

(19) Liu, S.; Zhang, Q.; Tian, X.; Fan, S.; Huang, J.; Whiting, A. Highly selective halogenation of unactivated C(sp3)−H with NaX under co-catalysis of visible light and Ag@AgX. *Green Chem.* **2018**, *20* (20), 4729−4737.

(20) Düsel, S. J. S.; König, B. Oxidative Photochlorination of Electron-Rich Arenes via in situ Bromination. *Eur. J. Org Chem.* **2020**, *2020* (10), 1491−1495.

(21) Bonciolini, S.; Noël, T.; Capaldo, L. Synthetic Applications of Photocatalyzed Halogen-Radical Mediated Hydrogen Atom Transfer for C−H Bond Functionalization. *Eur. J. Org Chem.* **2022**, *2022* (34), No. e202200417.

(22) Lin, R.; Amrute, A. P.; Perez-Ramirez, J. Halogen-Mediated Conversion of Hydrocarbons to Commodities. *Chem. Rev.* **2017**, *117* (5), 4182−4247.

(23) Rohe, S.; Morris, A. O.; McCallum, T.; Barriault, L. Hydrogen Atom Transfer Reactions via Photoredox Catalyzed Chlorine Atom Generation. *Angew. Chem., Int. Ed.* **2018**, *57* (48), 15664−15669.

(24) Xu, P.; Chen, P. Y.; Xu, H. C. Scalable Photoelectrochemical Dehydrogenative Cross-Coupling of Heteroarenes with Aliphatic C-H Bonds. *Angew. Chem., Int. Ed. Engl.* **2020**, *59* (34), 14275−14280.

(25) Deng, H. P.; Zhou, Q.; Wu, J. Microtubing-Reactor-Assisted Aliphatic C-H Functionalization with HCl as a Hydrogen-Atom-Transfer Catalyst Precursor in Conjunction with an Organic Photoredox Catalyst. *Angew. Chem., Int. Ed. Engl.* **2018**, *57* (39), 12661−12665.

(26) Yang, Q.; Wang, Y. H.; Qiao, Y.; Gau, M.; Carroll, P. J.; Walsh, P. J.; Schelter, E. J. Photocatalytic C-H activation and the subtle role of chlorine radical complexation in reactivity. *Science* **2021**, *372* (6544), 847−852.

(27) Panetti, G. B.; Yang, Q.; Gau, M. R.; Carroll, P. J.; Walsh, P. J.; Schelter, E. J. Discovery and mechanistic investigation of photo-induced sp3 C−H activation of hydrocarbons by the simple anion hexachlorotitanate. *Chem Catal.* **2022**, *2* (4), 853−866.

(28) Ohkubo, K.; Fujimoto, A.; Fukuzumi, S. Metal-free oxygenation of cyclohexane with oxygen catalyzed by 9-mesityl-10-methylacridinium and hydrogen chloride under visible light irradiation. *Chem. Commun.* **2011**, *47* (30), 8515−8517.

(29) Hirscher, N. A.; Ohri, N.; Yang, Q.; Zhou, J.; Anna, J. M.; Schelter, E. J.; Goldberg, K. I. A Metal-Free, Photocatalytic Method for Aerobic Alkane Iodination. *J. Am. Chem. Soc.* **2021**, *143* (46), 19262−19267.

(30) Gygi, D.; Gonzalez, M. I.; Hwang, S. J.; Xia, K. T.; Qin, Y.; Johnson, E. J.; Gygi, F.; Chen, Y. S.; Nocera, D. G. Capturing the Complete Reaction Profile of a C-H Bond Activation. *J. Am. Chem. Soc.* **2021**, *143* (16), 6060−6064.

(31) Gonzalez, M. I.; Gygi, D.; Qin, Y.; Zhu, Q.; Johnson, E. J.; Chen, Y. S.; Nocera, D. G. Taming the Chlorine Radical: Enforcing Steric Control over Chlorine-Radical-Mediated C-H Activation. *J. Am. Chem. Soc.* **2022**, *144* (3), 1464−1472.

(32) Shields, B. J.; Doyle, A. G. Direct C(sp ^{3})−H Cross Coupling Enabled by Catalytic Generation of Chlorine Radicals. *J. Am. Chem. Soc.* **2016**, *138* (39), 12719−12722.

(33) Wang, Y.-H.; Yang, Q.; Walsh, P. J.; Schelter, E. J. Light-mediated aerobic oxidation of C(sp3)−H bonds by a Ce(iv) hexachloride complex. *Org. Chem. Front.* **2022**, *9* (10), 2612−2620.

(34) Li, Z.; Luo, L.; Li, M.; Chen, W.; Liu, Y.; Yang, J.; Xu, S. M.; Zhou, H.; Ma, L.; Xu, M.; Kong, X.; Duan, H. Photoelectrocatalytic C-H halogenation over an oxygen vacancy-rich TiO(2) photoanode. *Nat. Commun.* **2021**, *12* (1), 6698.

(35) Deetz, A. M.; Troian-Gautier, L.; Wehlin, S. A. M.; Piechota, E. J.; Meyer, G. J. On the Determination of Halogen Atom Reduction Potentials with Photoredox Catalysts. *J. Phys. Chem. A* **2021**, *125* (42), 9355−9367.

(36) Adriaenssens, L.; Gil-Ramírez, G.; Frontera, A.; Quiñonero, D.; Escudero-Adán, E. C.; Ballester, P. Thermodynamic Characterization of Halide−π Interactions in Solution Using "Two-Wall" Aryl Extended Calix[4]pyrroles as Model System. *J. Am. Chem. Soc.* **2014**, *136* (8), 3208−3218.

(37) Tsao, M.-L.; Hadad, C. M.; Platz, M. S. Computational Study of the Halogen Atom−Benzene Complexes. *J. Am. Chem. Soc.* **2003**, *125* (27), 8390−8399.

(38) Walling, C. The transient species in radical chlorination in benzene solvent. *J. Org. Chem.* **1988**, *53* (2), 305−308.

(39) Raner, K. D.; Lusztyk, J.; Ingold, K. U. Ultraviolet/visible spectra of halogen molecule/arene and halogen atom/arene.pi.-molecular complexes. *J. Phys. Chem.* **1989**, *93* (2), 564−570.

(40) Benson, S. W. Some observations on the.pi.-complex of chlorine atoms with benzene. *J. Am. Chem. Soc.* **1993**, *115* (15), 6969−6974.

(41) Förgeteg, S.; Bérces, T. Laser flash photolysis study of chlorine atom/simple arene π-complexes in carbon tetrachloride and acetonitrile. *J. Photochem. Photobiol., A* **1993**, *73* (3), 187−195.

https://doi.org/10.1021/acs.inorgchem.4c01726
Inorg. Chem. 2024, 63, 15772−15783

(42) Isse, A. A.; Lin, C. Y.; Coote, M. L.; Gennaro, A. Estimation of standard reduction potentials of halogen atoms and alkyl halides. *J. Phys. Chem. B* **2011**, *115* (4), 678−684.
(43) Stanbury, D. Reduction Potentials Involving Inorganic Free Radicals in Aqueous Solution. *Adv. Inorg. Chem.* **1989**, *33*, 69−138.
(44) Schwarz, H. A.; Bielski, B. H. J. Reactions of hydroperoxo and superoxide with iodine and bromine and the iodide (I2-) and iodine atom reduction potentials. *J. Phys. Chem.* **1986**, *90* (7), 1445−1448.
(45) Schwarz, H. A.; Dodson, R. W. Equilibrium between hydroxyl radicals and thallium(II) and the oxidation potential of hydroxyl(aq). *J. Phys. Chem.* **1984**, *88* (16), 3643−3647.
(46) Wardman, P. Reduction Potentials of One-Electron Couples Involving Free Radicals in Aqueous Solution. *J. Phys. Chem. Ref. Data* **1989**, *18* (4), 1637−1755.
(47) Armstrong, D. A.; Huie, R. E.; Lymar, S.; Koppenol, W. H.; Merényi, G.; Neta, P.; Stanbury, D. M.; Steenken, S.; Wardman, P. Standard electrode potentials involving radicals in aqueous solution: inorganic radicals. *Bioinorg. React. Mech.* **2013**, *9* (1−4), 59−61.
(48) Du, J.; Chen, Z.; Chen, C.; Meyer, T. J. A half-reaction alternative to water oxidation: chloride oxidation to chlorine catalyzed by silver ion. *J. Am. Chem. Soc.* **2015**, *137* (9), 3193−3196.
(49) Gale, P. A.; Caltagirone, C. Anion sensing by small molecules and molecular ensembles. *Chem. Soc. Rev.* **2015**, *44* (13), 4212−4227.
(50) Hein, R.; Beer, P. D.; Davis, J. J. Electrochemical Anion Sensing: Supramolecular Approaches. *Chem. Rev.* **2020**, *120* (3), 1888−1935.
(51) Hua, Y.; Flood, A. H. Click chemistry generates privileged CH hydrogen-bonding triazoles: the latest addition to anion supramolecular chemistry. *Chem. Soc. Rev.* **2010**, *39* (4), 1262−1271.
(52) Gunnlaugsson, T.; Glynn, M.; Tocci née Hussey, G. M.; Kruger, P. E.; Pfeffer, F. M. Anion recognition and sensing in organic and aqueous media using luminescent and colorimetric sensors. *Coord. Chem. Rev.* **2006**, *250* (23−24), 3094−3117.
(53) Wade, C. R.; Broomsgrove, A. E.; Aldridge, S.; Gabbai, F. P. Fluoride ion complexation and sensing using organoboron compounds. *Chem. Rev.* **2010**, *110* (7), 3958−3984.
(54) Beer, P. D.; Dent, S. W.; Hobbs, G. S.; Wear, T. J. Novel anion binding selectivity trends exhibited by new dinuclear rhenium(i), ruthenium(ii) and osmium(ii) bipyridyl cleft-type receptors. *Chem. Commun.* **1997**, No. 1, 99−100.
(55) Beer, P. D.; Szemes, F.; Balzani, V.; Salà, C. M.; Drew, M. G. B.; Dent, S.; Maestri, M. Anion Selective Recognition and Sensing by Novel Macrocyclic Transition Metal Receptor Systems. 1H NMR, Electrochemical, and Photophysical Investigations. *J. Am. Chem. Soc.* **1997**, *119* (49), 11864−11875.
(56) Beer, P. D.; Fletcher, N. C.; Wear, T. Halide anion recognition by new acyclic ruthenium(II) bipyridyl-polypyridinium receptors. *Inorg. Chim. Acta* **1996**, *251* (1−2), 335−340.
(57) Uppadine, L. H.; Beer, P. D.; Drew, M. G. B. Anion selectivity properties of ruthenium(ii) tris(5,5′-diamide-2,2′-bipyridine) receptors dictated by solvent and amide substituent. *Chem. Commun.* **2001**, No. 3, 291−292.
(58) Cametti, M.; Rissanen, K. Recognition and sensing of fluoride anion. *Chem. Commun.* **2009**, No. 20, 2809−2829.
(59) Brunetti, E.; Picron, J. F.; Flidrova, K.; Bruylants, G.; Bartik, K.; Jabin, I. Fluorescent chemosensors for anions and contact ion pairs with a cavity-based selectivity. *J. Org. Chem.* **2014**, *79* (13), 6179−6188.
(60) Beer, P. D.; Gale, P. A. Anion Recognition and Sensing: The State of the Art and Future Perspectives. *Angew. Chem., Int. Ed. Engl.* **2001**, *40* (3), 486−516.
(61) Evans, N. H.; Beer, P. D. Advances in anion supramolecular chemistry: from recognition to chemical applications. *Angew. Chem., Int. Ed. Engl.* **2014**, *53* (44), 11716−11754.
(62) Werber, J. R.; Osuji, C. O.; Elimelech, M. Materials for next-generation desalination and water purification membranes. *Nat. Rev. Mater.* **2016**, *1* (5), 16018.
(63) Bisson, A. P.; Lynch, V. M.; Monahan, M. K. C.; Anslyn, E. V. Recognition of Anions through NHπ Hydrogen Bonds in a Bicyclic Cyclophane—Selectivity for Nitrate. *Angew Chem. Int. Ed. Engl.* **1997**, *36* (21), 2340−2342.
(64) Lau, Y. H.; Rutledge, P. J.; Watkinson, M.; Todd, M. H. Chemical sensors that incorporate click-derived triazoles. *Chem. Soc. Rev.* **2011**, *40* (5), 2848−2866.
(65) Bondy, C. R.; Loeb, S. J. Amide based receptors for anions. *Coord. Chem. Rev.* **2003**, *240* (1−2), 77−99.
(66) Liu, Y.; Zhao, W.; Chen, C. H.; Flood, A. H. Chloride capture using a C-H hydrogen-bonding cage. *Science* **2019**, *365* (6449), 159−161.
(67) Zahran, E. M.; Fatila, E. M.; Chen, C. H.; Flood, A. H.; Bachas, L. G. Cyanostar: C-H Hydrogen Bonding Neutral Carrier Scaffold for Anion-Selective Sensors. *Anal. Chem.* **2018**, *90* (3), 1925−1933.
(68) Troian-Gautier, L.; Beauvilliers, E. E.; Swords, W. B.; Meyer, G. J. Redox Active Ion-Paired Excited States Undergo Dynamic Electron Transfer. *J. Am. Chem. Soc.* **2016**, *138* (51), 16815−16826.
(69) Brynn Hibbert, D.; Thordarson, P. The death of the Job plot, transparency, open science and online tools, uncertainty estimation methods and other developments in supramolecular chemistry data analysis. *Chem. Commun.* **2016**, *52* (87), 12792−12805.
(70) Thordarson, P. Determining association constants from titration experiments in supramolecular chemistry. *Chem. Soc. Rev.* **2011**, *40* (3), 1305−1323.
(71) Thordason, P. Supramolecular.org. http://app.supramolecular.org/bindfit/ (accessed June 1, 2022).
(72) Connelly, N. G.; Geiger, W. E. Chemical Redox Agents for Organometallic Chemistry. *Chem. Rev.* **1996**, *96* (2), 877−910.
(73) Crosby, G. A.; Demas, J. N. Measurement of photoluminescence quantum yields. Review. *J. Phys. Chem.* **1971**, *75* (8), 991−1024.
(74) Rohwer, L. S.; Martin, J. E. Measuring the absolute quantum efficiency of luminescent materials. *J. Lumin.* **2005**, *115* (3−4), 77−90.
(75) Bard, A. J.; Faulkner, L. R. *Electrochemical Methods: Fundamentals and Applications*, 2nd ed.; Wiley: New York, 2001.
(76) Rehm, D.; Weller, A. Kinetik und Mechanismus der Elektronübertragung bei der Fluoreszenzlöschung in Acetonitril. *Ber. Bunsenges. Phys. Chem.* **1969**, *73* (8−9), 834−839.
(77) Lakowicz, J. R. *Principles of Fluorescence Spectroscopy*, 3rd ed.; Kluwer Academic/Plenum: New York, 2006.
(78) Deetz, A. M.; Meyer, G. J. Resolving Halide Ion Stabilization through Kinetically Competitive Electron Transfers. *JACS Au* **2022**, *2* (4), 985−995.
(79) Marton, A.; Clark, C. C.; Srinivasan, R.; Freundlich, R. E.; Narducci Sarjeant, A. A.; Meyer, G. J. Static and Dynamic Quenching of Ru(II) Polypyridyl Excited States by Iodide. *Inorg. Chem.* **2006**, *45* (1), 362−369.
(80) Deetz, A. M.; Goodwin, M. J.; Kober, E. A.; Meyer, G. J. Nanosecond Intra-Ionic Chloride Photo-Oxidation. *Inorg. Chem.* **2023**, *62* (29), 11414−11425.
(81) Ward, W. M.; Farnum, B. H.; Siegler, M.; Meyer, G. J. Chloride ion-pairing with Ru(II) polypyridyl compounds in dichloromethane. *J. Phys. Chem. A* **2013**, *117* (36), 8883−8894.
(82) Turlington, M. D.; Deetz, A. M.; Vitt, D.; Meyer, G. J. Photocatalyst assemblies with two halide ions. *J. Photochem. Photobiol.* **2022**, *9*, 100090.
(83) Turlington, M. D.; Troian-Gautier, L.; Sampaio, R. N.; Beauvilliers, E. E.; Meyer, G. J. Ligand Control of Supramolecular Chloride Photorelease. *Inorg. Chem.* **2018**, *57* (9), 5624−5631.
(84) Szemes, F.; Hesek, D.; Chen, Z.; Dent, S. W.; Drew, M. G. B.; Goulden, A. J.; Graydon, A. R.; Grieve, A.; Mortimer, R. J.; Wear, T.; Weightman, J. S.; Beer, P. D. Synthesis and Characterization of Novel Acyclic, Macrocyclic, and Calix[4]arene Ruthenium(II) Bipyridyl Receptor Molecules That Recognize and Sense Anions. *Inorg. Chem.* **1996**, *35* (20), 5868−5879.
(85) Liu, Y.; Sengupta, A.; Raghavachari, K.; Flood, A. H. Anion Binding in Solution: Beyond the Electrostatic Regime. *Chem* **2017**, *3* (3), 411−427.

https://doi.org/10.1021/acs.inorgchem.4c01726
Inorg. Chem. 2024, 63, 15772−15783

(86) Curiel, D.; Beer, P. D.; Paul, R. L.; Cowley, A.; Sambrook, M. R.; Szemes, F. Halide anion directed assembly of luminescent pseudorotaxanes. *Chem. Commun.* **2004**, *10*, 1162−1163.
(87) Millan, G.; Nieddu, M.; Lopez, I. P.; Ezquerro, C.; Berenguer, J. R.; Larrayoz, I. M.; Pichel, J. G.; Lalinde, E. A new family of luminescent iridium complexes: synthesis, optical, and cytotoxic studies. *Dalton Trans.* **2023**, *52* (19), 6360−6374.
(88) Ion, L.; Morales, D.; Nieto, S.; Perez, J.; Riera, L.; Riera, V.; Miguel, D.; Kowenicki, R. A.; McPartlin, M. Biimidazole and bis(amide)bipyridine molybdenum carbonyl complexes as anions receptors. *Inorg. Chem.* **2007**, *46* (7), 2846−2853.
(89) Caltagirone, C.; Mulas, A.; Isaia, F.; Lippolis, V.; Gale, P. A.; Light, M. E. Metal-induced pre-organisation for anion recognition in a neutral platinum-containing receptor. *Chem. Commun.* **2009**, No. 41, 6279−6281.
(90) Rowley, J. G.; Farnum, B. H.; Ardo, S.; Meyer, G. J. Iodide Chemistry in Dye-Sensitized Solar Cells: Making and Breaking I−I Bonds for Solar Energy Conversion. *J. Phys. Chem. Lett.* **2010**, *1* (20), 3132−3140.
(91) Pavlishchuk, V. V.; Addison, A. W. Conversion constants for redox potentials measured versus different reference electrodes in acetonitrile solutions at 25°C. *Inorg. Chim. Acta* **2000**, *298* (1), 97−102.
(92) De Kreijger, S.; Elias, B.; Troian-Gautier, L. Chloride, Bromide, and Iodide Photooxidation in Acetonitrile/Water Mixtures Using Binuclear Iridium(III) Photosensitizers. *Inorg. Chem.* **2023**, *62* (39), 16196−16202.
(93) De Kreijger, S.; Ripak, A.; Elias, B.; Troian-Gautier, L. Investigation of the Excited-State Electron Transfer and Cage Escape Yields Between Halides and a Fe(III) Photosensitizer. *J. Am. Chem. Soc.* **2024**, *146* (15), 10286−10292.
(94) Englman, R.; Jortner, J. The energy gap law for radiationless transitions in large molecules. *Mol. Phys.* **1970**, *18* (2), 145−164.
(95) Levich, V. G. *Physical Chemistry: An Advanced Treatise*. Eyring, H., Henderson, D., Eds.; Vol. *9B*; Academic Press, 1970.
(96) Damrauer, N. H.; Boussie, T. R.; Devenney, M.; McCusker, J. K. Effects of Intraligand Electron Delocalization, Steric Tuning, and Excited-State Vibronic Coupling on the Photophysics of Aryl-Substituted Bipyridyl Complexes of Ru(II). *J. Am. Chem. Soc.* **1997**, *119* (35), 8253−8268.
(97) Kestner, N. R.; Logan, J.; Jortner, J. Thermal electron transfer reactions in polar solvents. *J. Phys. Chem.* **1974**, *78* (21), 2148−2166.

https://doi.org/10.1021/acs.inorgchem.4c01726
Inorg. Chem. 2024, 63, 15772−15783